

Supplemental Information

β -Barrel Mobility Underlies Closure

of the Voltage-Dependent Anion Channel

Ulrich Zachariae, Robert Schneider, Rodolfo Briones, Zrinka Gattin, Jean-Philippe Demers, Karin Giller, Elke Maier, Markus Zweckstetter, Christian Griesinger, Stefan Becker, Roland Benz, Bert L. de Groot, and Adam Lange

Inventory of Supplemental Information

Figure S1: Lipid bilayer measurements on WT-hVDAC1 and the deletion mutant $\Delta(1-20)$ -hVDAC1; related to Figures 4E, F, and 5.

Figure S2: (^{13}C , ^{13}C) correlation spectra recorded on the three hVDAC1 variants investigated; related to Figures 4A and B.

Figure S3: Potentials of mean force for cations and anions in the mVDAC1 pore; related to Figure 3B.

Figure S4: (^{13}C , ^{13}C) side-chain cross-peak volume ratios between L10N- and WT-hVDAC1 spectra; related to Figure 4C.

Table S1: Values of S_{CC} order parameters as displayed in Figure 1.

Supplemental Experimental Procedures.

Supplemental Data

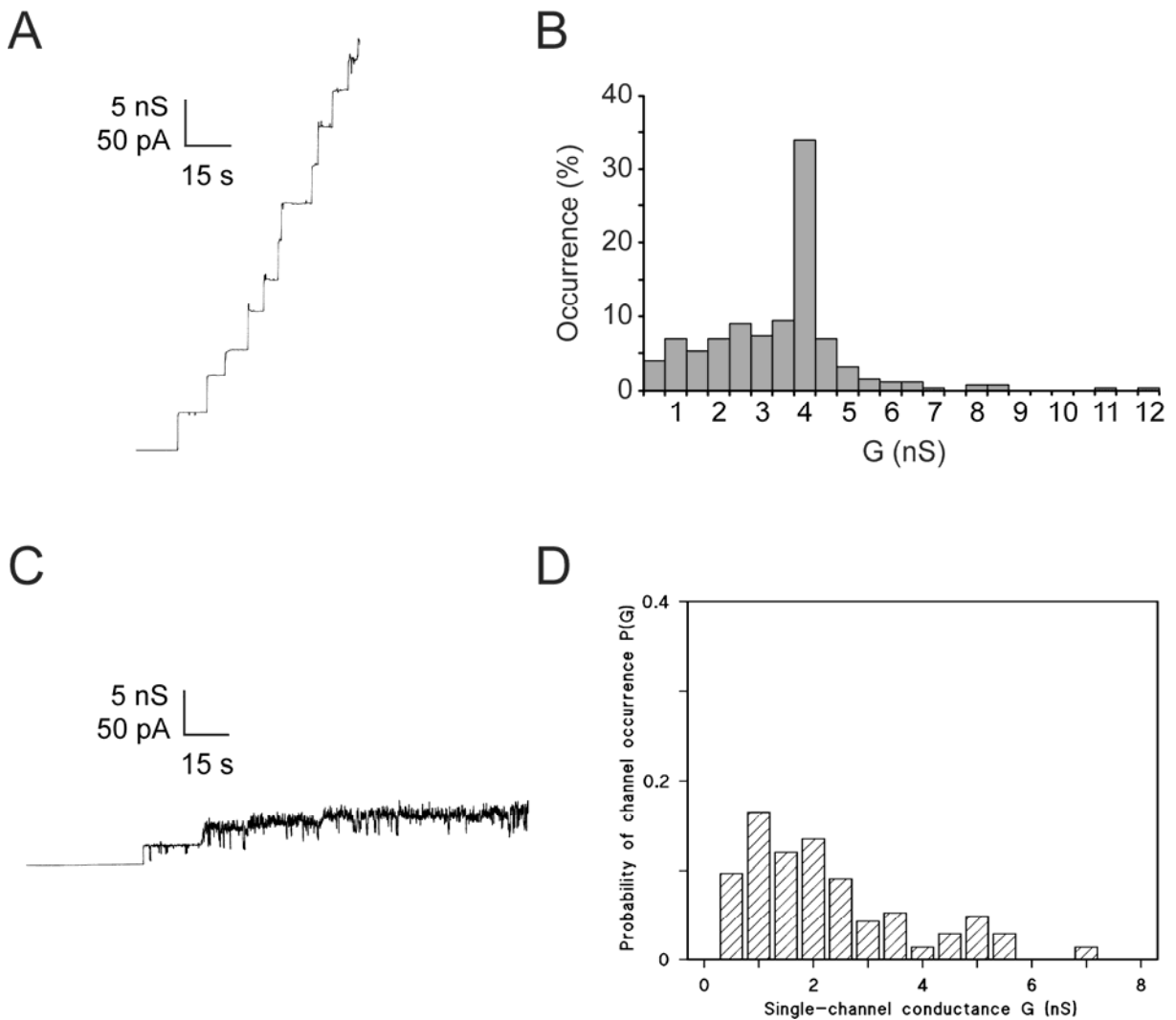


Figure S1, related to Figures 4E, F, and 5: Lipid bilayer measurements on WT-hVDAC1 and on the deletion mutant $\Delta(1-20)$ -hVDAC1. (A) Single-channel recording of insertions of WT-hVDAC1. (B) Histogram of observed WT-hVDAC1 conductance (G) values at a transmembrane voltage of 10 mV. The open state conductance of 4 nS is predominantly observed. (C) Single-channel recording of insertions of $\Delta(1-20)$ -hVDAC1. (D) Histogram of observed $\Delta(1-20)$ -hVDAC1 conductance (G) values at a transmembrane voltage of 10 mV.

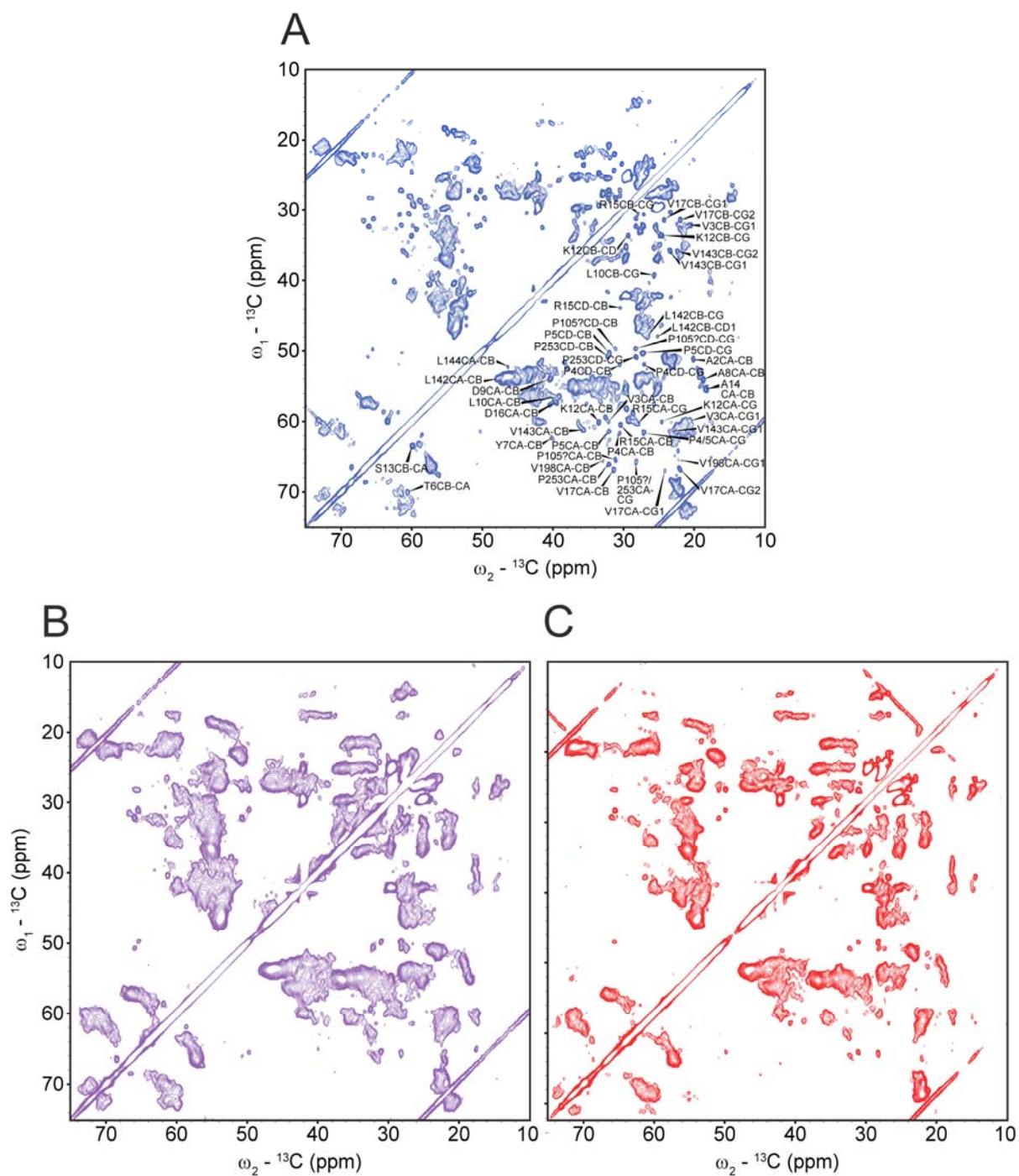


Figure S2, related to Figures 4A and B: Aliphatic region of $(^{13}\text{C}, ^{13}\text{C})$ proton-driven spin diffusion (PDS) spectra recorded on the three hVDAC1 variants investigated: (A) wild-type-, (B) L10N-, and (C) $\Delta(1-20)$ -hVDAC1. Panel (A) also shows assignments as obtained in ref. (Schneider et al., 2010a). All spectra were processed identically and recorded at 20.0 T, +5°C sample temperature, and a magic-angle spinning (MAS) frequency of 10.6 kHz, using 15 ms of PDS mixing, except the spectrum in (C) for which 20 ms mixing and 11 kHz MAS were used.

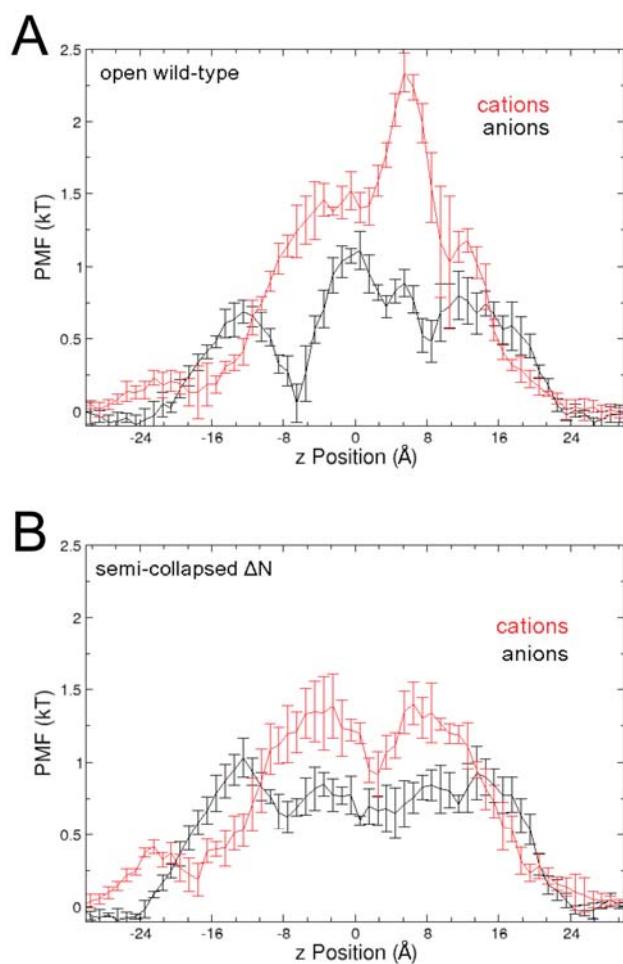


Figure S3, related to Figure 3B: Potentials of mean force (PMF) for cations and anions traversing the mVDAC1 pore. The z axis corresponds to the membrane normal; its zero point was chosen at the center of mass of the molecule. (A) WT-mVDAC1 in the open state. The peak in the cation curve corresponds to the positively charged N-terminal helix (B) $\Delta(1-20)$ -mVDAC1 in the semi-collapsed state.

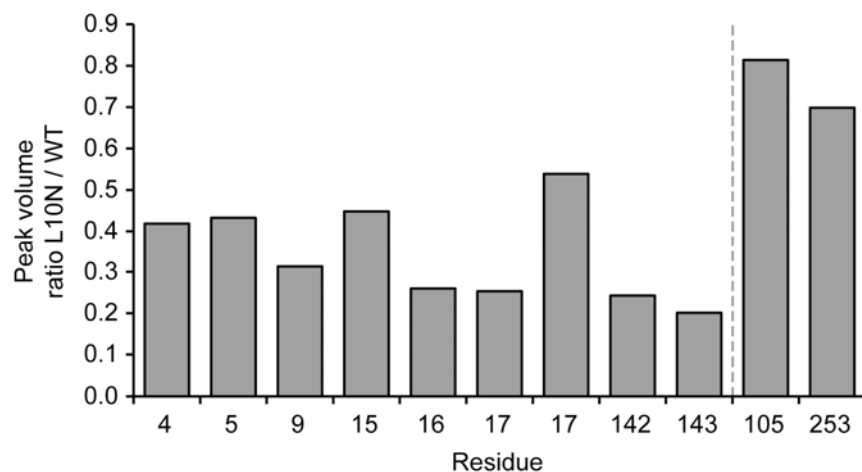


Figure S4, related to Figure 4C: Ratios of normalized C β -C γ side-chain cross-peak volumes between ($^{13}\text{C}, ^{13}\text{C}$) PDS spectra (15 ms mixing time) recorded on L10N- and WT-hVDAC1. In L10N-hVDAC1, these signals are more attenuated in N-terminus and β -strand 9 than in control residues 105 and 253 ($p = 0.0253$, two-sided t-test, unequal variances assumed), as is the case for C α -C β cross-peaks (Fig. 4C in the main text). The two bars for residue Val17 refer to C β -C γ 1 and C β -C γ 2 correlations.

Residue	S_{CC}	S_{CC} error
A2	0.85	0.02
V3	-	-
P4	1.00	0.03
P5	0.85	0.04
T6	0.80	0.02
Y7	-	-
A8	0.90	0.10
D9	1.00	0.01
L10	0.80	0.02
G11	-	-
K12	0.95	0.04
S13	0.95	0.04
A14	0.95	0.01
R15	0.80	0.10
D16	0.98	0.05
V17	0.88	0.05
L144	0.80	0.02
Ala β	0.95	0.00
Leu β	0.88	0.05
Thr β	0.90	0.10
Val β	0.80	0.10
β 1	0.83	0.05
β 2	0.83	0.05
Lys SC	0.58	0.05

Table S1: Values of S_{CC} order parameters as displayed in Figure 1 in the main text. All values are measured on $C\alpha$ - $C\beta$ correlations except the value for lysine sidechains (“Lys SC”) which was measured on lysine $C\delta$ - $C\epsilon$ correlations. See Supplemental Experimental Procedures for details.

Supplemental Experimental Procedures

Solid-state NMR

Initial ^1H - ^{13}C cross-polarization (CP) time was set to 600 μs . Typical proton field strength for 90° pulses and SPINAL64 (Fung et al., 2000) decoupling was 83 kHz. ^{13}C - ^{13}C mixing was accomplished by proton-driven spin diffusion (PDS) for 15 ms, using a MAS frequency of 10.6 kHz at a static field of 20.0 T. Double quantum – single quantum (2Q,1Q) correlation spectra were recorded using a ^{13}C field strength of 40 kHz at 8 kHz MAS and a static field of 18.8 T. Six different spectra with excitation and reconversion times each of 250, 400, 500, 600, 750, or 1000 μs were recorded.

Evaluation of (2Q,1Q) spectra for obtaining order parameters was done using custom-written scripts in MATLAB (The MathWorks, Natick, MA, USA) after importing processed spectra using the MatNMR (van Beek, 2007) add-on package. Cross-peak volumes were integrated to yield build-ups of cross-peak intensity. To extract order parameters from these, simulated build-ups for different order parameters (i.e. scaling factors of the dipolar ^{13}C - ^{13}C coupling) were generated in an amino acid type-specific way using the GAMMA C++ program library (Smith et al., 1994) as described in ref. (Schneider et al., 2010b) and fit to the experimental build-ups using chi-square minimization. The order parameter used in the simulation yielding the smallest chi-square value in the fit was taken to be the order parameter of the corresponding experimental build-up. Data for which no good fits could be obtained (defined as a correlation coefficient between experimental data and simulation of less than 0.9 or a correlation coefficient between 0.9 and 0.95 together with a chi-square value above 20) were excluded from the analysis. Errors of order parameters were estimated based on Monte Carlo simulations, where estimates of the experimental error were obtained from absolute values of integrals in spectral noise regions, scaled by the size of the respective signal integration region. Extracted order parameters for build-ups that report on mobility of the same bond (e.g. CACB-CA and CACB-CB) were averaged if they differed, using standard error propagation or the difference of the two values, whichever was greater, as the error of the average.

For determining relative signal intensities in spectra of WT- and L10N-hVDAC1, PDS spectra with 15 ms mixing time acquired and processed in the same fashion were used. Signal intensities were measured by integration of cross-peaks in Topspin (Bruker Biospin, Karlsruhe, Germany). For each signal in each spectrum, values from symmetry-related cross-peaks on both sides of the diagonal were added and normalized to the average value of four integrals within the same spectrum, using regions with large signal intensities containing overlapping resonances from

different residue types (Ser and Leu C α -C β as well as Lys C γ -C δ and C δ -C ϵ resonances) to avoid systematic intensity variations in the signals used for normalization. Thus, only relative cross-peak intensities normalized within each spectrum were compared between spectra. This approach excluded effects of overall spectral intensity differences due to, e.g., differing amounts of labeled protein or different cross-polarization efficiencies. Cross-peaks exhibiting strong overlap with other signals were excluded from this analysis. This applied also to resonances Ala8 and Ala14, which appear well resolved in (^{13}C , ^{13}C) PDSB spectra, but overlap with signals from outside the N-terminus, as can be seen in spectra from $\Delta(1-20)$ -hVDAC1 where spectral intensity can still be found at these positions. Signals that vanish in the spectrum of L10N-hVDAC1 (Tyr7, Leu144) were also excluded. Figures 4C and S4 show the ratios between these normalized peak intensity values between the two spectra.

For determining linewidths of cross-peaks, the same PDSB spectra of WT- and L10N-hVDAC1 were used as for measuring signal intensities. Linewidths were measured using the command 'pe' in Sparky (T. D. Goddard and D. G. Kneller, SPARKY 3, University of California, San Francisco) and averaged over both spectral dimensions and both cross-peaks on each side of the diagonal. Only resolved cross-peaks were used. Values shown in Figure 4D are ratios between these averaged linewidth values in the two spectra.

Electrophysiology

The membrane current was measured with a Keithley 427 current amplifier. The amplified signal was monitored with a storage oscilloscope and recorded on a strip chart recorder. hVDAC1 and its mutants were added to one or both sides of the membranes because there was no obvious asymmetry of the pores. The channel-forming activity of the proteins was approximately the same.

The probability $P(G)$ for the occurrence of a given conductivity unit in single-channel experiments (Figs. 4F, S1B, and S2B) was calculated by dividing the number of fluctuations with a given conductance increment by the total number of conductance fluctuations. The applied membrane potential was 10 mV. Histograms were derived from at least 100 conductance steps. For voltage-dependence measurements, the refolded recombinant hVDAC1 was added at a concentration of about 100 ng/ml to one or both sides of a black diphytanoyl-phosphatidylcholine/n-decane membrane. After about 20 min the reconstitution of porin channels into the membrane reached equilibrium. Then, different potentials were applied to the cis-side of the membrane starting with ± 10 mV. These experiments were repeated with ± 20 to ± 80 mV in steps of ± 10 mV.

The experiments were analyzed as follows: the membrane conductance (G) as a function of voltage,

V_m , was measured when the opening and closing of channels reached an equilibrium, i.e. after the exponential decay of the membrane current following the voltage step V_m . G was divided by the initial value of the conductance (G_0 , which was a linear function of the voltage) obtained immediately after the onset of the voltage. The data of Fig. 5 correspond to the symmetric voltage-dependence of WT-hVDAC1, the mutant L10N-hVDAC1, and the N-terminal deletion mutant $\Delta(1-20)$ -hVDAC1 (mean \pm SD of three membranes).

Molecular Dynamics Simulations

Electrostatic interactions were calculated explicitly at a distance smaller than 1.0 nm, long-range electrostatic interactions were treated by particle-mesh Ewald summation at every step (Darden et al., 1993). Lennard-Jones interactions were calculated using a cutoff of 1.0 nm. Water bond distances and angles were constrained using SETTLE (Miyamoto and Kollman, 1992). The LINCS algorithm was employed to constrain all protein and lipid bonds (Hess et al., 1997). The simulation temperature was kept constant by weakly ($t = 0.1$ ps) coupling the system to a temperature bath of 320 K using the velocity rescale method (Bussi et al., 2007). The pressure was kept constant by semi-isotropic Berendsen coupling of the system to a pressure bath of 1 bar, separately for the xy- and for the z-direction (Berendsen et al., 1984). By employing a virtual sites model (Berendsen et al., 1999), an integration time-step of 4 fs was used. The combination of force-field and water model was selected based on the results of Hess and van der Vegt (Hess and van der Vegt, 2006). The protonation states of titratable residues of VDAC, especially that of the Glu73 side chain which points towards the lipid bilayer, were determined by Monte Carlo sampling (Beroza and Case, 1996) based on results from Poisson-Boltzmann calculations using MEAD (Bashford and Gerwert, 1992). According to these calculations, a neutral Glu73 side chain is most probable at pH 7. Therefore, we used the protonated form of Glu73 in our simulations ($E73^0$).

The ellipticity of the barrels was calculated by fitting an ellipse to the barrel C α atoms in the x-y plane after alignment along the z axis according to the ratio $(b-a)/a$, where b and a are the minor and major axes of the ellipse, respectively.

For simulations of ion flux by computational electrophysiology (Kutzner et al., 2011), transmembrane voltages were applied using a small charge imbalance across two lipid bilayers containing WT or mutant VDAC and separating two aqueous compartments, formed by duplication of the systems described in the main text. The deterministic ion-interchange scheme as described in (Kutzner et al., 2011) was used. Conductance and selectivity were calculated from the channel cation and anion flux within 20-ns time slices. The transmembrane potential was determined by solving the Poisson equation during the same time windows, imposing equal voltage at the z

boundaries of the simulation box (Tieleman and Berendsen, 1996). Values were averaged over the two channels.

In simulations of isotropic membrane surface tension, the pressure in the xy-plane was increased to 150 bar, while that in z direction was kept at 1 bar. This corresponds to a membrane surface tension of -45 mN/m. To model anisotropic membrane stress, a uniaxial pressure of 40 bar was applied in either x or y direction. Force probe simulations mimicking the effect of an electric field of $\sim 6.7 \times 10^8$ V/m on the N-terminal helix, carrying a surplus of two positive charges, were performed by exerting a constant force of 120 pN on the C α atom of sequence position 10, chosen as it is located halfway between the N-terminus of WT-VDAC1 and the $\Delta(1-20)$ -deletion.

Supplemental References

Bashford, D., and Gerwert, K. (1992). Electrostatic calculations of the pKa values of ionizable groups in bacteriorhodopsin. *J Mol Biol* 224, 473-486.

Berendsen, H.J.C., Feenstra, K.A., and Hess, B. (1999). Improving efficiency of large time-scale molecular dynamics simulations of hydrogen-rich systems. *J. Comput. Chem.* 20, 786-798.

Berendsen, H.J.C., Postma, J.P.M., Vangunsteren, W.F., Dinola, A., and Haak, J.R. (1984). Molecular dynamics with coupling to an external bath. *J. Chem. Phys.* 81, 3684-3690.

Beroza, P., and Case, D.A. (1996). Including side chain flexibility in continuum electrostatic calculations of protein titration. *J. Phys. Chem.* 100, 20156-20163.

Bussi, G., Donadio, D., and Parrinello, M. (2007). Canonical sampling through velocity rescaling. *J Chem Phys* 126, 014101.

Darden, T., York, D., and Pedersen, L. (1993). Particle Mesh Ewald - an N.Log(N) method for Ewald sums in large systems. *J. Chem. Phys.* 98, 10089-10092.

Fung, B.M., Khitritin, A.K., and Ermolaev, K. (2000). An improved broadband decoupling sequence for liquid crystals and solids. *J. Magn. Reson.* 142, 97-101.

Hess, B., Bekker, H., Berendsen, H.J.C., and Fraaije, J.G.E.M. (1997). LINCS: A linear constraint solver for molecular simulations. *J. Comput. Chem.* 18, 1463-1472.

Hess, B., and van der Vegt, N.F.A. (2006). Hydration thermodynamic properties of amino acid analogues: A systematic comparison of biomolecular force fields and water models. *J. Phys. Chem. B* 110, 17616-17626.

Kutzner, C., Grubmüller, H., de Groot, B.L., and Zachariae, U. (2011). Computational electrophysiology: the molecular dynamics of ion channel permeation and selectivity in atomistic detail. *Biophys J* 101, 809-817.

Miyamoto, S., and Kollman, P.A. (1992). Settle - an analytical version of the Shake and Rattle algorithm for rigid water models. *J. Comput. Chem.* 13, 952-962.

Schneider, R., Eitzkorn, M., Giller, K., Daebel, V., Eisfeld, J., Zweckstetter, M., Griesinger, C., Becker, S., and Lange, A. (2010a). The native conformation of the human VDAC1 N terminus. *Angew Chem Int Ed Engl* 49, 1882-1885.

Schneider, R., Seidel, K., Etkorn, M., Lange, A., Becker, S., and Baldus, M. (2010b). Probing molecular motion by double-quantum ($^{13}\text{C},^{13}\text{C}$) solid-state NMR spectroscopy: application to ubiquitin. *J Am Chem Soc* *132*, 223-233.

Smith, S.A., Levante, T.O., Meier, B.H., and Ernst, R.R. (1994). Computer simulations in magnetic resonance. An object-oriented programming approach. *Journal of Magnetic Resonance, Series A* *106*, 75-105.

Tieleman, D.P., and Berendsen, H.J.C. (1996). Molecular dynamics simulations of a fully hydrated dipalmitoyl phosphatidylcholine bilayer with different macroscopic boundary conditions and parameters. *J. Chem. Phys.* *105*, 4871-4880.

van Beek, J.D. (2007). matNMR: A flexible toolbox for processing, analyzing and visualizing magnetic resonance data in Matlab((R)). *J. Magn. Reson.* *187*, 19-26.